

Ion expansion characteristics from a KrF-laser-produced plasma

P. D. Gupta,* Y. Y. Tsui, R. Popil, R. Fedosejevs, and A. A. Offenberger

Department of Electrical Engineering, University of Alberta, Edmonton, Alberta, Canada T6G 2G7

(Received 30 September 1985)

Two groups of ions are observed in an aluminum plasma produced by focusing a Raman-compressed KrF-laser beam (268 nm) on thick planar targets in the intensity range 5×10^{11} – 10^{13} W/cm². The angular distribution, velocity distribution, energy partition between the two groups, and scaling of the ion velocities with laser intensity are presented. The role of lateral energy transport in generating the two groups of ions is discussed.

The study of ion expansion characteristics in laser-produced plasmas plays an important role in understanding the physical processes involved in ablation^{1–3} and in determining ablation parameters.^{4–6} The observation of a single sharp peak in the velocity distribution of ions is taken as a signature of steady-state ablation.¹ The occurrence of a second group of faster ions generated by wave particle interactions in the plasma is observed at high laser intensities, particularly for long wavelength irradiation.^{2,3} Recently, there has been a great emphasis on using short wavelength lasers for plasma ablation to enhance collisional absorption⁷ and to achieve higher ablation rates^{5,6} and hydrodynamic efficiency.⁸ It has therefore become important to characterize the ion expansion in such plasmas.

In this paper, we present a study of the ion expansion characteristics of an aluminum plasma created by focusing a Raman-compressed KrF-laser beam on planar targets in the intensity range of 10^{11} – 10^{13} W/cm². Ablation studies in this intensity range using an upconverted Nd:glass laser system have been reported previously.⁶ However, no detailed characterization of the ion features was given. In particular, we report the occurrence of two-peak behavior observed on ion current traces and measurements of angular distributions, velocity distributions, and energy partition between these two groups of ions and the scaling of ion velocities with laser intensity. The origin of the two ion groups is discussed in terms of lateral heat-flow effects in the plasma.

The experiments were performed using 2-ns duration [full width at half maximum (FWHM)] Raman-compressed⁹ KrF-laser pulses¹⁰ at 268 nm with energies of up to 1 J on target. The laser pulse was focused onto a massive aluminum planar target using a planoconvex 700-mm-focal-length quartz lens. The focal-spot intensity distribution was monitored on every shot using an equivalent focal-plane imaging system coupled to a uv video digitizer system. At best focus the 50% and 90% energy contours have areas corresponding to equivalent diameters of 34 and 74 μ m, respectively. The effective laser intensity was calculated using 90% of the energy and the area of the 90% energy contour. The pulse shape was measured with a high-speed streak camera and the energy with a pyroelectric calorimeter. The intensity was varied by changing the laser energy. Lower intensities were also obtained by moving the lens toward the target by 2- and 4-mm distances. The equivalent 90% energy containing diameters for these conditions were 170 and 340 μ m, respectively.

Arrays of plasma calorimeters¹¹ and Faraday cups¹² were used to map the angular distribution of energy and ion velocity in the expanding plasma. The differential calorime-

ters were calibrated by depositing a known amount of energy in resistors embedded in the aluminum absorption plates. A 25- μ m-thick Mylar sheet in front of one of the calorimeter elements of each pair blocked all scattered uv light, ions, and soft x rays. The output was measured as the difference of the signals from the two elements of the calorimeter, one of which measured background, thus eliminating the effect of any thermal drift inside the interaction chamber on the measurements. The Faraday cups were deep metallic cylindrical cups placed behind a pair of grids, one of which was biased to -90 V and the other kept at ground potential. The zero time reference was obtained by displaying the laser pulse signal, as observed by a photodiode on the same measurement channel during calibration shots.

The ion current traces observed in a direction $\theta = 14^\circ$ with respect to the target normal for different laser intensities are shown in Fig. 1. In the intensity range of 5×10^{11} – 10^{13} W/cm² for best-focus and for 2-mm out-of-focus irradiation, the ion current traces show a two-peak behavior as seen in Figs. 1(c)–1(f). It is observed that the first peak becomes increasingly dominant with increasing laser intensi-

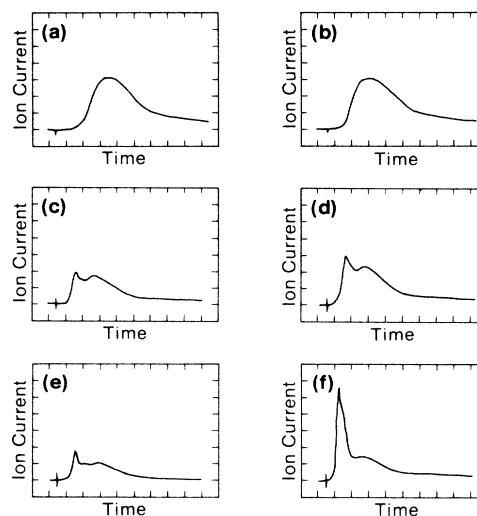


FIG. 1. Ion current traces observed in a direction of 14° with respect to target normal. The laser intensities for (a)–(f) are 1.2×10^{11} , 3.7×10^{11} , 6.7×10^{11} , 1.1×10^{12} , 2.7×10^{12} , and 7.1×10^{12} W/cm², respectively. The 90% energy containing diameters of the focal spots are (a) and (b) 340 μ m, (c) and (d) 174 μ m, and (e) and (f) 74 μ m. Magnitude of each division on the vertical scale on trace (b) is twice that of all other traces. The time scale is 50 ns/div.

ty. As the direction of observation is changed, the second peak becomes relatively more prominent with increasing values of θ as shown in Fig. 2. For smaller laser intensity in the large-focal-spot irradiation, only one peak was observed, although its FWHM is quite broad (Fig. 1).

Ion velocities corresponding to the two peaks were observed to be quite different, both in magnitude and in their scaling with laser intensity I_L . For the best-focus irradiation at a laser intensity of 5×10^{12} W/cm², the peak velocities of the two groups of ions observed for $\theta = 14^\circ$ are 3×10^7 cm/sec and 1.1×10^7 cm/sec, respectively. Furthermore, for best-focus irradiation, the scaling of the velocity obtained from the first peak is $I_L^{0.26}$, which is in good agreement with the $I_L^{0.22-0.25}$ expected from a self-regulating model.¹³ On the other hand, the second peak velocity scales much slower—proportional to $I_L^{0.08}$. For the lowest-intensity large-focal-spot irradiation, the peak velocity scales as $I_L^{0.22}$, which is again close to that expected from the self-regulating model.

The total energy measured by the plasma calorimeters was obtained by integrating over the measured angular distribution. In the intensity range of 10^{12} – 10^{13} W/cm² for best-focus irradiation, the measured plasma energy accounted for $88 \pm 15\%$ of the incident laser energy. The uncertainty includes the error in the energy calibration of the calorimeters' response and the shot-to-shot variations in the data. Half of this energy was contained in a cone angle of 45° . Measurements of the scattered light using an Ulbricht sphere showed that $(97 \pm 2)\%$ of the incident laser energy was absorbed. While the agreement between the energy calorimeters and the Ulbricht sphere results is within the error bars, the somewhat lower ion calorimeter values may be due to loss of energy because of secondary emission from the calorimeter surface, particularly for low-energy ions.¹⁴

An insight into the two-peak behavior can be obtained by calculating the velocity distributions from the ion current traces. The velocity distribution of ions at the detector is essentially governed by the hydrodynamic expansion of the hot plasma in vacuum where the initial thermal energy is converted to kinetic energy. However, recombination occurring during expansion alters the charge state of ions.^{15,16} Knowledge of the variation of the charge state of ions with velocity in the expanding plasma is therefore required to determine the velocity distribution of ions from the ion current traces.

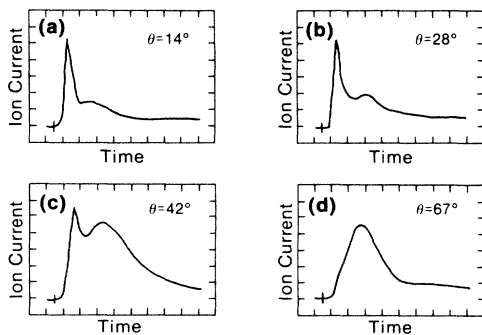


FIG. 2. Ion current traces observed in different directions with respect to target normal for best-focus irradiation at 7.1×10^{12} W/cm². Magnitude of each division on the vertical scale of the traces (b), (c), and (d) is smaller by factors of 1.5, 4.5, and 10, respectively, as compared to that for the trace (a).

Studies of the charge state of ions as a function of velocity has been reported by various authors.^{17,18} In aluminum plasma produced by using 1.06- and 0.53- μ m laser radiation, Leppelmeier, Wilson, and Morse¹⁷ have observed that the average ion charge Z_i increases linearly with velocity, and this dependence does not vary appreciably with laser intensity, wavelength, target thickness, or its orientation. In fact, a single dependence of Z_i on velocity fitted all the data for different directions of observation. Similar observations have also been made by Bykovskii *et al.*,¹⁸ who found that Z_i as a function of velocity did not change with laser intensity. In view of this, we analyze the present results using a charge dependence of

$$Z_i = 4.5 + 2.2[v/(10^7 \text{ cm/sec}) - 2.0] \quad (1)$$

for the velocity range of $(1-5) \times 10^7$ cm/sec, based on the results of Ref. 17 and using $Z_i = 11$ for $v > 5 \times 10^7$ cm/sec. To check the applicability of this relation for our case, the energy of the ions per unit solid angle was computed from the ion current traces using Eq. (1). The resulting energies were found to be in very good agreement with the corresponding calorimetric data for all the angles of observation.

The ion velocity distributions corresponding to the ion current traces (b), (d), and (f) of Fig. 1 are shown in Fig. 3. The velocities corresponding to the peaks of current traces are also indicated by arrows. It is seen that for the high-intensity best-focus irradiation, the ion velocity distribution shows a plateau region which lies between the velocities corresponding to the two ion peaks. At lower intensities the length of the plateau region decreases. Furthermore, the velocity distribution in the region of the second peak fits a straight line on the semilog plot, which is typical of an isothermal expansion.¹⁹ For the low-intensity large-focal-spot irradiation, the velocity distribution does not show any plateau region.

Estimates of the relative energy content of ions of the two peaks were obtained by splitting the current traces into two overlapping peaks, such that their sum represents the observed ion trace. The kinetic energy and the momentum normal to the target of the ions were then computed using

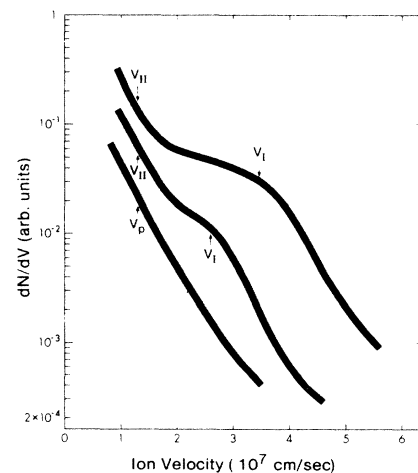


FIG. 3. Ion velocity distributions corresponding to the traces of Fig. 1: (b), (d), (f) (bottom, middle, top, respectively). The relative displacement on the vertical scale for these distributions is only for sake of clarity. The velocities corresponding to the peaks of the ion traces are indicated by the arrows.

Eq. (1). The resultant angular distributions of these for the case of best-focus irradiation at a laser energy of 0.85 J are shown, as an example, in Fig. 4. It is observed that whereas ions in the first peak are emitted preferentially closer to the target normal, ions in the second peak show a more isotropic distribution. Angular integration of the energy revealed that the ion energy in the first peak increases with laser intensity, reaching 50% of the total for the maximum laser intensity of the experiment.

The possibility of ions in the first peak being protons due to an impurity layer of hydrocarbon on the target surface under irradiation can be ruled out. If we integrate the current in the first peak and use $Z_i=1$ (for protons), the estimated thickness of the layer would be $1\ \mu\text{m}$ which is much more than the thickness of contamination expected for a clean target surface. This was confirmed by comparing the ion current signals observed from a fresh target surface to those observed when the target surface was heated prior to irradiation. The preheating was done by firing ten shots of defocused laser beam to give an energy density of $\sim 10\ \text{J}/\text{cm}^2$, sufficient to evaporate the surface layers. No significant change in the two-peak behavior of signals was observed.

For the laser intensities and wavelength of the present study, a highly collisional plasma is expected. For a laser intensity of $10^{13}\ \text{W}/\text{cm}^2$ at $\lambda_L=268\ \text{nm}$, typical parameters of the absorption region predicted from a self-regulating model¹³ are $T_e=330\ \text{eV}$, $n_e=4.5\times 10^{21}\ \text{cm}^{-3}$, $Z_i=11$. This gives an electron-ion collision time $\tau_{ei}=8.5\times 10^{-15}\ \text{sec}$, which is much smaller than the typical plasma flow time ($t_f=R/c_s$, R =focal-spot radius, and c_s =sound speed) of 0.3 ns. The plasma is thus highly collisional and the threshold intensities for most parametric processes^{20,21} would be well above $10^{13}\ \text{W}/\text{cm}^2$. Experimental measurements²² of x-ray continuum intensity showed a single temperature spectrum in agreement with the self-regulating model. Further, no detectable x-ray emission for $h\nu\geq 10\ \text{keV}$ was observed, indicating a negligible level of any hot electron generation at the present intensities.

For long wavelength irradiation, the onset of thermal conduction inhibition in moderate Z plasma has been observed at intensities above $10^{14}\ \text{W}/\text{cm}^2$, whereas classical thermal conduction is sufficient to describe measurements made

below $10^{13}\ \text{W}/\text{cm}^2$.^{14,23,24} Therefore, no significant inhibition of thermal conduction is expected for the intensities in our experiment. Self-generated magnetic fields would also not be expected to have any significant effect in modifying energy transport. At the maximum intensity of $10^{13}\ \text{W}/\text{cm}^2$ for best-focus irradiation, assuming $T_e=330\ \text{eV}$, $\theta=45^\circ$, $\Delta t=1\ \text{ns}$, and a temperature scale length of the order of the focal-spot radius, the thermoelectric generated magnetic field is 1.7 MG.²⁵ The product of electron cyclotron frequency ω_{ce} and τ_{ei} is 0.25, which is smaller than 1.

A number of possible explanations for the two-peak behavior are easily eliminated. A slower ion component is sometimes inferred to be due to the plasma arising from shock heating in the target.¹ However, the estimated ion energy of the second peak is $\geq 50\%$ of the total, which is much too high compared to the energy expended in the shock. According to simple estimates, the latter is given by $\frac{1}{2}\sqrt{\rho/\rho_0}$, where ρ is the density of the absorption region and ρ_0 is that of the ablating solid.²⁶ In the present case, this number is estimated to be only $\sim 3\%$. In addition, the energy of the ions in the second peak ($\sim 1\text{--}3\ \text{keV}$) and the electron temperature ($\sim 50\text{--}100\ \text{eV}$) estimated from the slope of the velocity distribution in the region of the second peak (Fig. 3) are both too high to correspond to the shock heated plasma. The laser light incident on the target outside of the main focal-spot region contains only 10% of the total energy, and thus could not produce the slow ion component. The laser pulse also contains a significant temporal modulation depth ($\sim 50\%$) on a 200–400-ps time scale. However, shots taken with varying pulse shapes and varying degree of modulation all gave similar ion current traces. Thus, there is no observable dependence on the pulse modulation.

The observed two-peak behavior can be qualitatively explained by considering lateral heat conduction in the plasma. When a laser beam irradiates a planar target, initially a local region of hot plasma is formed. Due to the high temperature in this plasma, thermal diffusion is important. The scale length for thermal diffusion L_T is given by $\sqrt{4Dt}$, where D is the thermal diffusivity and t is the time to establish the steady flow pattern. When $L_T > R$, one would expect the heated zone to increase in radius until it reaches a dimension of the order of L_T .^{27,28} However, the increased effective size of the heated region results in a smaller temperature, which in turn makes further diffusion less important.²⁹ This results in a steady-state three-dimensional (3D) flow structure in the plasma with an effective size larger than the initial focal spot. The plasma ablated in this state would have characteristics corresponding to a reduced effective laser intensity. Under these conditions, a transition is expected from the initial high-temperature flow to a lower-temperature steady-state flow. On the other hand, if the initial focal-spot size is much larger than L_T , the flow will remain essentially 1D.

The thermal diffusion length can be estimated for the typical parameters of our experiment. For a laser intensity of $10^{13}\ \text{W}/\text{cm}^2$ at best focus, $T_e=330\ \text{eV}$, $n_e=4.5\times 10^{21}\ \text{cm}^{-3}$, $Z_i=11$, the thermal diffusion length is $\approx 100\ \mu\text{m}$, which is much larger than the focal spot radius of $37\ \mu\text{m}$. Thus, by considering thermal conduction, lateral energy flow would certainly be very important for best-focus ($R=37\text{-}\mu\text{m}$) and the 2-mm out-of-focus ($R=87\text{-}\mu\text{m}$) conditions and less important for the 4-mm out-of-focus ($R=170\text{-}\mu\text{m}$) condition.

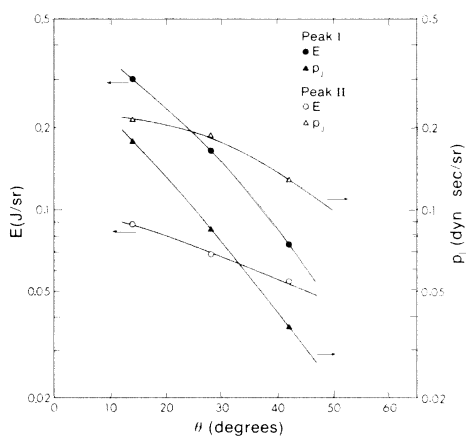


FIG. 4. Angular distribution of kinetic energy and momentum in the two ion peaks for the best-focus irradiation. The laser energy on the target is 0.85 J.

It is necessary, however, to include energy dissipation due to ablation in the periphery, which would have the effect of reducing the size of the heated region. An estimate of this modified thermal conduction length can be obtained by comparing the lateral thermal conduction heat flux to the outward convective energy flow in a manner similar to Ref. 27. By balancing the thermal heat flux KT_e/L_T over a conduction length of L_T , where K is the heat conductivity, and the convective flow of energy in the periphery of the plasma, $3 m_i n_i c_s^3$, where m_i is the ion mass and n_i is the ion density, the conduction length is estimated to be $\sim 54 \mu\text{m}$ for an average temperature in the periphery which is half that in the central region.

We would expect the actual heated zone to lie somewhere between the above two limits; a detailed 2D numerical calculation would be required to obtain a more accurate scale length.

Thus, the ions in the first peak correspond to the initial hot ablating plasma still undergoing 1D flow, while those in the second peak correspond to the 3D plasma flow occurring over an effectively larger area. The plateau region in the velocity distribution would correspond to the transition from 1D to 3D flow. This picture is consistent with the following experimental observations: (1) The angular distribution of kinetic energy and momentum observed for the first ion peak is confined to a narrow cone around target normal, while those for the second ion peak are rather isotropic, consistent with the spherical flow developing later in time, after lateral spread has occurred; (2) the time required to establish steady-state flow is determined by L_T/c_s . Since $L_T \sim T_e^{5/4}$ and $c_s \sim T_e^{1/2}$, the time increases with increasing temperature and laser intensity. Therefore, the transition period will be longer at higher intensity consistent with the increased extent of the plateau region observed in the ion velocity distribution. (3) The first-peak velocity scales as

$I_L^{0.26}$, in agreement with the predictions of a self-regulating model. The second peak scales much slower as $I_L^{0.08}$, in agreement with that derived in Ref. 27 for strong lateral conduction. A slower scaling is expected because the incident laser energy for the second ion peak is shared over an area which is increasing with laser intensity. (4) X-ray streak pictures observed for best focus irradiation showed that the x-ray emission ($h\nu > 1 \text{ keV}$) occurs over a significantly smaller duration of time than the incident laser pulse, corresponding to the initial period of hot ablating plasma. In addition, the flow pattern for the second ion peak is observed to correspond to an isothermal expansion which is established as a result of thermal diffusion dominating.

In summary, we have presented a study of ion expansion characteristics in aluminum plasma produced by a KrF laser. Two groups of ions observed from the two-peak behavior are qualitatively consistent with lateral energy transport predictions. However, as pointed out earlier, 2D numerical simulations are required for a more detailed quantitative analysis of the laser-plasma interaction. A substantial fraction of the total ion energy is estimated to be invested in the slower group of ions, and the first group of ions does not show a sharp peak in the velocity distribution, as expected from a steady-state ablation. Thus, a careful analysis of the ion measurements is required in order to properly determine ablation parameters such as ablation velocity or mass ablation rate.

The authors would like to acknowledge the technical assistance of B. Harwood and K. Houston throughout the course of these experiments, and express thanks for the loan of detectors from Dr. A. Ng of the University of British Columbia. This research was supported by the Natural Sciences and Engineering Research Council of Canada.

*On leave from Bhabha Atomic Research Centre, 400085 Bombay, Maharashtra, India.

¹J. P. Anthes, M. A. Gusinow, and M. K. Matzen, Phys. Rev. Lett. **41**, 1300 (1978).

²S. Sakabe, T. Mochizuki, T. Tabe, K. Mima, and C. Yamanaka, Phys. Rev. A **26**, 2159 (1982).

³P. Church, F. Martin, H. Pepin, and R. Decoste, J. Appl. Phys. **53**, 874 (1982).

⁴M. H. Key, W. T. Toner, T. J. Goldsack, J. D. Kilkenny, S. A. Veats, P. F. Cunningham, and C. L. S. Lewis, Phys. Fluids **26**, 2011 (1983).

⁵R. Fabbro, E. Fabre, F. Amiranoff, C. Garban-Labaune, J. Virmont, and M. Weinfeld, Phys. Rev. A **26**, 2289 (1982).

⁶A. Ng, D. Pasini, P. Celliers, D. Parfeniuk, L. DaSilva, and J. Kwan, Appl. Phys. Lett. **45**, 1046 (1984).

⁷C. Garban-Labaune, E. Fabre, C. E. Max, R. Fabbro, F. Amiranoff, J. Virmont, M. Weinfeld, and A. Michard, Phys. Rev. Lett. **48**, 1018 (1982).

⁸C. E. Max and K. G. Estabrook, Comments Plasma Phys. Controlled Fusion **5**, 239 (1980).

⁹J. R. Murray, J. Goldhar, D. Eimerl, and A. Szoke, IEEE J. Quantum Electron. **QE-15**, 342 (1979).

¹⁰D. C. D. McKen, R. Fedosejevs, M. Arnfield, I. V. Tomov, C. Domier, and A. A. Offenberger, Rev. Sci. Instrum. **54**, 845 (1983).

¹¹D. M. Villeneuve and M. C. Richardson, Rev. Sci. Instrum. **51**, 306 (1980).

¹²I. Pelah, Phys. Lett. **59A**, 348 (1976).

¹³P. Mora, Phys. Fluids **25**, 1051 (1982).

¹⁴K. Eidmann, F. Amiranoff, R. Fedosejevs, A. G. M. Maaswinkel, R. Petsch, R. Sigel, G. Spindler, Y. Teng, G. Tsakiris, and S. Wit-

kowski, Phys. Rev. A **30**, 2568 (1984).

¹⁵R. R. Goforth and P. Hammerling, J. Appl. Phys. **47**, 3918 (1976).

¹⁶M. K. Matzen and J. S. Pearlman, Phys. Fluids **22**, 449 (1979).

¹⁷G. Leppelmeier, J. Wilson, and R. Morse, Laboratory for Laser Energetics, University of Rochester, Report No. 87, 1979 (unpublished).

¹⁸Yu. A. Bykovskii, N. N. Degtyarenko, V. F. Elesin, Yu. P. Kozzyrev, and S. M. Silnov, Zh. Eksp. Teor. Fiz. **60**, 1306 (1971) [Sov. Phys. JETP **33**, 706 (1971)].

¹⁹J. E. Crow, P. L. Auer, and J. E. Allen, J. Plasma Phys. **14**, 65 (1975).

²⁰C. S. Liu, in *Advances in Plasma Physics*, edited by A. Simon and W. B. Thompson (Wiley, New York, 1976), Vol. 6.

²¹W. B. Thompson, *Modern Plasma Physics* (IAEA, Vienna, 1981), IAEA Report No. SMR-61/113, 1981, p. 437.

²²P. D. Gupta, R. Popil, R. Fedosejevs, A. A. Offenberger, D. Salzmann, and C. E. Capjack, Appl. Phys. Lett. **48**, 103 (1986).

²³G. McClellan, P. H. Y. Lee, and G. Caporaso, Phys. Rev. Lett. **44**, 658 (1980).

²⁴J. Grun, S. P. Obenschain, B. H. Ripin, R. R. Whitlock, E. A. McLean, J. Gardner, M. J. Herbst, and J. A. Stamper, Phys. Fluids **26**, 588 (1983).

²⁵C. E. Max, W. M. Manheimer, and J. J. Thomson, Phys. Fluids **21**, 128 (1978).

²⁶C. G. M. van Kessel, Z. Naturforsch **30a**, 1581 (1975).

²⁷G. J. Pert, Plasma Phys. **16**, 1019 (1974).

²⁸C. L. S. Lewis, P. F. Cunningham, L. Pina, A. K. Roy, and J. M. Ward, J. Phys. D **15**, 69 (1982).

²⁹J. Grun, R. Decoste, B. H. Ripin, and J. Gardner, Appl. Phys. Lett. **39**, 545 (1981).